Journal of MATERIALS RESEARCH

Article
DOI:10.1557/s43578-022-00842-5

Reversible electrospun fibers containing spiropyran for acid and base vapor sensing

Flávio B. Miguez[1], Olívia B. O. Moreira[2], Marcone A. L. de Oliveira[2], Ângelo M. L. Denadai[3], Luiz F. C. de Oliveira[4], Frederico B. De Sousa[1,a)]

[1] Laboratório de Sistemas Poliméricos e Supramoleculares (LSPS)—Instituto de Física e Química, Universidade Federal de Itajubá (UNIFEI), Itajubá, MG 37500-903, Brazil
[2] Grupo de Química Analítica e Quimiometria (GQAQ)—Departamento de Química—ICE, Universidade Federal de Juiz de Fora (UFJF), Juiz de Fora, MG 36036-900, Brazil
[3] Instituto de Ciências da Vida (ICV), Universidade Federal de Juiz de Fora, Campus Governador Valadares (UFJF-GV), Governador Valadares, MG 35010-177, Brazil
[4] Núcleo de Espectroscopia E Estrutura Molecular—Departamento de Química—ICE, Universidade Federal de Juiz de Fora (UFJF), Juiz de Fora, MG 36036-900, Brazil
[a)] Address all correspondence to this author. e-mail: fredbsousa@gmail.com; fredbsousa@unifei.edu.br

Received: 7 July 2022; accepted: 15 November 2022; published online: 28 November 2022

Among the various possible structural modifications spiropyrans may be subject to, ones containing alkyl sulfonates groups are commonly classified as photoacids. Both alkyl sulfonates spiropyrans named SON and SOH were structurally characterized and their acido- and photochromic properties were studied by UV–visible spectroscopy. Electrospun poly-ε-caprolactone (PCL) fibers were obtained, in which SON or SOH were incorporated with the goal of detecting acid and base vapors. PCL fibers containing the derivatives SON and SOH were successfully obtained (0.8 µm range), capable of acting as colorimetric vapor sensors according to the acidochromic properties of the spiropyrans. PCL-SON fibers presented quick vapor sensing capability, with colorimetric change within 10 s of exposure. Scanning electronic microscopy was crucial to characterize the morphology of these fibers before and after being used in the sensing process. This material could be reversibly reutilized in the sensing of acids and bases vapors according to the results presented.

Introduction

Spiropyrans are part of an important class of organic molecules that exhibit chromic properties based on a vast variety of external stimuli. Like other chromic compounds, spiropyrans are capable of undergoing reversible structural isomerization, from a spiro (SP) closed-ring colorless (in solution) form to an open-ring colorful isomer with an extensive π-electron conjugated system often referred to as merocyanine (MC) [1, 2]. This class of molecules are usually well recognized for their photochromic properties, which entails radiation. In addition, other external stimuli that may be able to control the spiropyrans isomerization process also includes pH variation [3], solvent polarity [4], temperature [5], and mechanical stress [6]. Another distinguishable feature of spiropyrans compared to other well-known photochromic molecules, such as diarylethenes, fulgides, and azobenzenes, is the distinctive physicochemical properties of both isomers previously mentioned (SP and MC). Among the essential differences, the larger electric dipole moment and molecular volume of the MC when compared to the SP isomer can be emphasized [7, 8]. Furthermore, other properties based on spiropyran structures have been investigated in order to expand the molecule application.

Among these properties the proton transfer can be highlighted [9], by using metastable-state photoacid merocyanine derivatives as presented in Fig. 1. The equilibrium between protonated (SPH^+ and MCH^+) and deprotonated MC (SP and MC) isomers have been reported in the literature based on the pH values of aqueous solution [10]. Spiropyran derivatives containing a propyl sulfonated group could also undergo the ring-opening isomerization in low pH to form MCH^+, with a characteristic absorption band shifted toward shorter wavelengths, compared to MC, with the possibility of modulating the pH in aqueous media with light irradiation [11]. Figure 1 depicts the isomerization of spiropyran based on light irradiation and

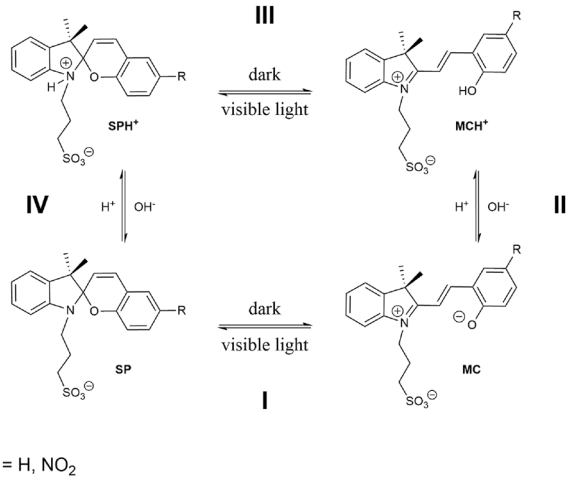

Figure 1: Equilibria in aqueous media among SP, SPH^+, MC, and MCH^+ isomers based on acid/base and/or light irradiation, for the SON and SOH species.

acid/base equilibrium. These spiropyran derivatives containing a propyl sulfonated group, with or without a nitro group at the benzopyran moiety are denominated in this work as SON and SOH, respectively.

In recent years, micro and nano stimulus-responsive systems have been constantly improving to a great degree, gaining considerable attention in the smart materials sciences community [12, 13]. These nanoscale systems have gained prominence in the technological growth and miniaturization of electronic devices. Ordinarily named "smart materials" have wider applications as sensors, optical memory devices, in the biomedical field, in self-sustained systems, among many others [14–20]. The ability to measure pH is required when determining a material's chemical properties and behavior. Controlling pH is critical to manage and prevent unwanted chemical reactions as well as optimizing desired beneficial reactions. Although glass electrode pH sensors can provide accurate, fast, and reliable measurement of pH, they also suffer from a few drawbacks, such as delicate materials, complex construction, which associates with high cost, and the need for frequent calibration [21].

Thus, responsive sensors for pH and acidic or basic vapors are of significant importance, as they allow for a visual change in the color of the substance in addition to a quick response [22]. Then, polymer devices containing chromic molecules are becoming more popular as a low-cost alternative to the well stablished, traditional analytical instruments [23, 24], which these materials could be assembled, for example, as films, composites, or fibers [21, 25]. Among these systems, fibers usually present a valuable advantage, a high surface area to volume ratio due to its low diameter. Genovese et al. compared systems consisting of films and fibers containing a spiropyran derivative as a gas detection for acetic and formic acid, observing a 25% reduction in response time for the fiber material compared to film, of the same composition [25]. Covalently bonding or incorporating spiropyrans in polymer matrixes may still increase photofatigue resistance, enhance switching rate and sensitivity [22, 26].

Herein, poly-ε-caprolactone (PCL), a biodegradable and easily-handled polyester [27], was electrospun into nanofibers containing two spiropyran derivatives, SOH or SON (respectively, PCL-SOH and PCL-SON). PCL electrospun fibers have demonstrated to be a great alternative for materials applied for chemical sensing and catalysis [28, 29]. This system was prepared as a fast approach for developing polymer-based sensors due to their high surface to volume ratio [29], which allows for faster responses and higher sensitivities by two or three orders of magnitude with respect to conventional films [25], verifying the acidochromic properties of the polymeric materials and their capability for sensing acid and base vapors. Moreover, electrospun materials color changing reversibility was explored. Structural and electronic characterization of SON and SOH, in solution and solid state, as well as their acido- and photochromic properties were also investigated.

Results and discussion

Structural characterization of spiropyrans and electrospun fibers

Both compounds (SON and SOH) were synthesized successfully, and their structures were analyzed by means of nuclear magnetic resonance (NMR), mass spectrometry (MS), and Raman spectroscopy. Figure S1a and b depicts the ^{1}H NMR spectra for SOH and SON, respectively, including their chemical structures inserted. Results corroborate data from the literature [30], and hydrogens' chemical shift attributions are presented in Table S1. Mass spectrometry analysis indicate the *m/z* 383.2 for [SOH–H^+], and *m/z* 431.1 for [SON + 2H^+] (Figure S2), which corroborate the structures presented in Fig. 1.

Raman spectra for all compounds are depicted in Fig. 2 (750–1750 cm^{-1}) and the main vibrational bands are discussed below (see Figure S3 for full spectra). Figure 2(a) and (b) present the spectra for SON and SOH, respectively; in both spectra it can be observed a band in the region between 1245 and 1270 cm^{-1} with the same intensity, assigned to the C–O–C stretching mode, very characteristic of aromatic ethers, present in the closed-ring isomer of the spiropyrans. Another very relevant band is related to the S–O stretching mode of sulfonated groups, this particular band is usually found in the 1165–1172 cm^{-1} region [31], in this study such band can be seen in the region 1180–1200 cm^{-1}, and this subtle change in wavenumber values can be due to the proximity of the nitrogen present in the five membered ring bonded to the alkyl sulfonate group. Small variations in the C–C stretching mode of aromatic rings give rise to strong bands seen at 1604 cm^{-1} for SON and 1591 cm^{-1} for SOH, this last vibrational band shows the shifting due to the presence of

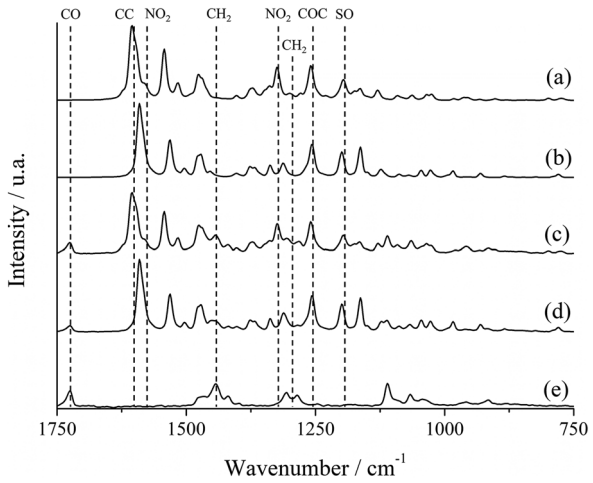

Figure 2: Raman spectra of: (a) SON, (b) SOH, (c) PCL-SON, (d) PCL-SOH, and (e) PCL from 750 to 1750 cm^{-1}.

NO_2 group in SON structure, an electron-withdrawing group which is responsible for such shift to higher wavenumber values. The NO_2 vibrational modes can be found only in the SON spectrum [Fig. 2(a)], the symmetrical stretching mode is found at 1315–1330 cm^{-1} region and asymmetrical stretching is found as a small shoulder of the C–C stretching discussed previously, at 1581 cm^{-1}.

As for the pure PCL fibers [Fig. 2(e)] it is important to highlight a few vibrational modes that are not seen in the spiropyrans spectra: first is the carbonyl group, C=O stretching, in the 1716–1740 cm^{-1} region, very characteristic band of this vibrational mode. Other important vibrational mode is the CH_2 bending of the methylene groups, which can be seen at 1442 cm^{-1}, as well the CH_2 twisting showing up as a doublet in the 1279–1319 cm^{-1} region. All PCL bands observed are in accordance with the literature [32]. These three vibrational modes are present in both polymer matrixes, PCL-SON and PCL-SOH, and can be observed in Fig. 2(c) and (d), respectively. The remaining bands observed in the spectra of these fibers can be assigned to their corresponding spiropyran group, discussed previously, with no significant shift for the vibrational modes.

Acidochromic characterization of spiropyrans

Apart from structural characterization, UV–visible absorption spectroscopy was carried out to study the spiropyrans, in solution, with respect to their acidochromic property, Fig. 3. Differently to most spiropyrans, SOH and SON are water-soluble and present color immediately after solubilization [11], meaning that merocyanines isomers (MC and MCH^+) may be favored, such as presented in the equilibrium shown in Fig. 1.

Figure 3(a) depicts the UV–visible spectra of SOH in aqueous solutions, at pH 2.2 it is expected to find mostly MCH^+ species, which is characterized by a large band with its peak at 424 nm. On the other hand, at pH close to the equivalent point (pH 7.5) and at alkaline medium (pH 11.5) it is possible to note the appearance of a new band at 534 nm, traditionally attributed to MC isomer which is in equilibrium with MCH^+. The same solutions were irradiated with visible light for a 5 min period [Fig. 3(b)], for the solution at pH 2.2 we note a significant decrease in the absorbance of its main visible band at 424 nm. This behavior is common among sulfonated spiropyrans as described in the literature in which SP and SPH^+ species may be observed [10]. Furthermore, at neutral pH a similar phenomenon, as for acidic medium, is observed. Contrary to the discussion above, at high pH levels, visible radiation does not seem to affect the equilibrium between all MC and SP species, described in Fig. 1. For the SON photoacid [Fig. 3(c)], at pH 2.2, MCH^+ band can also be found at 407 nm, slightly dislocated when compared to the same system in SOH, mainly due to the presence of an electron-withdrawing NO_2 group in the phenolate moiety of the molecule. In the same spectrum we highlight a band at 315 nm, which has been assigned to a *cis*-MCH^+ isomer [11]. As was discussed for SOH, at higher pH levels, SON also presents bands related to both MC and MCH^+ isomers, with maximum absorptions at 366 nm (pH 7.5) and 388 nm (pH 11.5). For all different pH solutions with SON, visible light dislocates the equilibrium to completely favor the SP or SPH^+ isomers. Specifically for high pH levels, SON and SOH display different behaviors related to visible light influence, which may be attributed to the NO_2 group.

In addition to the UV–visible analysis, potentiometric, conductometric, and zeta-potential acid–base titrations have been performed for each spiropyran, in order to provide further understanding of the factors that affect the equilibrium between MCH^+, MC, and SP or SPH^+ species. Equivalence point for SOH was found at pH 6.5 and for SON at pH 6.6, being in accordance to other data in the literature regarding pKa and pH of photoacids [30]. Figure 4(a) and (b) show the potentiometric titrations, where can be observed the usual sigmoidal profile, from acid regime to the basic regime, upon titration with NaOH. Figure 4(a) and (b) (insert) also point out the color changes upon increasing of pH. Given what can be observed in the color changes as pH is increased, SOH not only could be used in solution as a pH indicator to differentiate acidic and basic environments, but to also contrast smaller variations. With a highly acidic pH the color of SOH starts as a bright yellow and goes to a light shade of orange at pH 5.3, it darkens until it reaches a neutral pH, which then turns to pink in an alkaline medium. The same behavior is not seen in SON with the same colorimetric sensibility, which has an electron-withdrawing group (NO_2) in the benzopyran moiety. Under absence of light irradiation (dark conditions) derivative spiropyrans have demonstrated different pH values change, based on the electron-withdrawing NO_2 group on the phenol moiety [33].

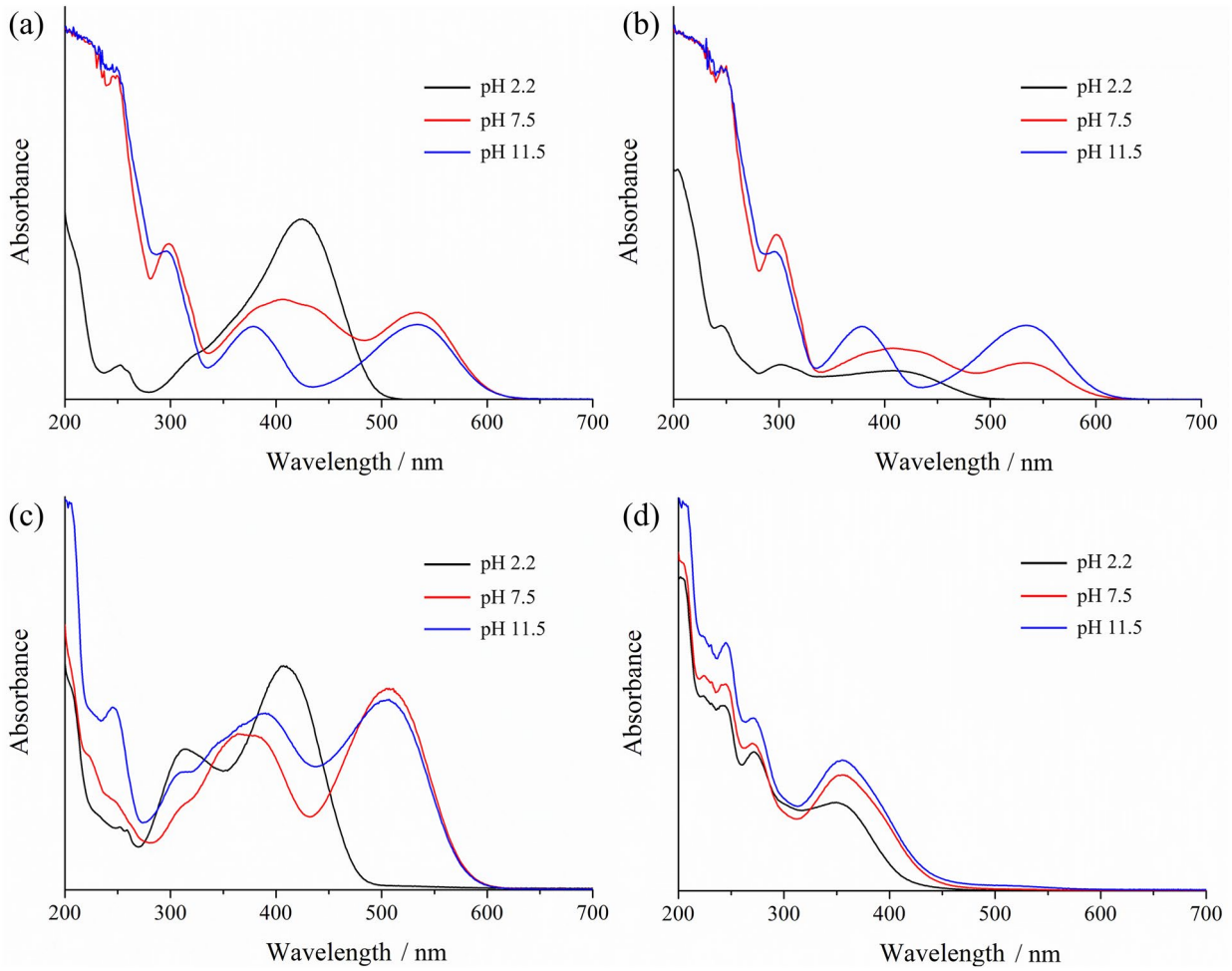

Figure 3: UV–visible spectra in aqueous solutions of SOH (a) under dark conditions and (b) after 5 min of visible light exposure, and SON (c) under dark conditions and (d) after 5 min of visible light exposure.

Electrical conductivity (k) is a non-selective property that reflects the global ionic concentration of a given solution. Figure 4(c) and (d) show that the curves exhibited a typical conductometric profile similar to those of the acid–base titrations, where the curve could be divided into two branches. The first and descending section, was characterized by the reaction between OH^- anions with free H^+ cations, beyond deprotonation of cationic SOH or SON. The second section of the curve, which an increasing in the conductivity was observed, being characterized by the increase of free OH^- and Na^+ during titration. At the minimal of curves, the equivalence point is observed.

Finally, the effect of NaOH titration in the ionized and solvated SOH and SON was monitored by zeta potential (ZP) titrations [Fig. 4(e, f)]. As can be observed, the spiropyran showed an initial positive ZP, due to the protonated state. However, during titration, the ZP values remain relatively constant until the equivalence point, from which occur an expressive decrease in the ZP values. This reduction occurs crossing the isoelectric point, that is, the point of NaOH concentration (or pH) where ZP = 0. Once again it is possible observe that equivalence point is slightly lower for SON than SOH, which has been attributed to the mesomeric effect caused by NO_2 in SON, give rising a more stable conjugated base.

Electrospun PCL fibers containing spiropyrans

Based on the acidochomic properties previously described in solution for the SOH and SON, electrospun fibers were successfully obtained in order to make possible the practical applications of the acidochromic spiropyrans, and the scanning electron microscopy (SEM) images are presented in Fig. 5. Both fibers are shown to have a distinct cylindrical shape without undesired morphological aspects such as beads or drops. In addition, no photochromic properties of SON and SOH were observed for these derivatives when incorporated into polymer matrices, similar behavior was described in literature for other spiropyran derivative in solid matrixes [34, 35]. The diameters for both systems were measured and found a distribution of

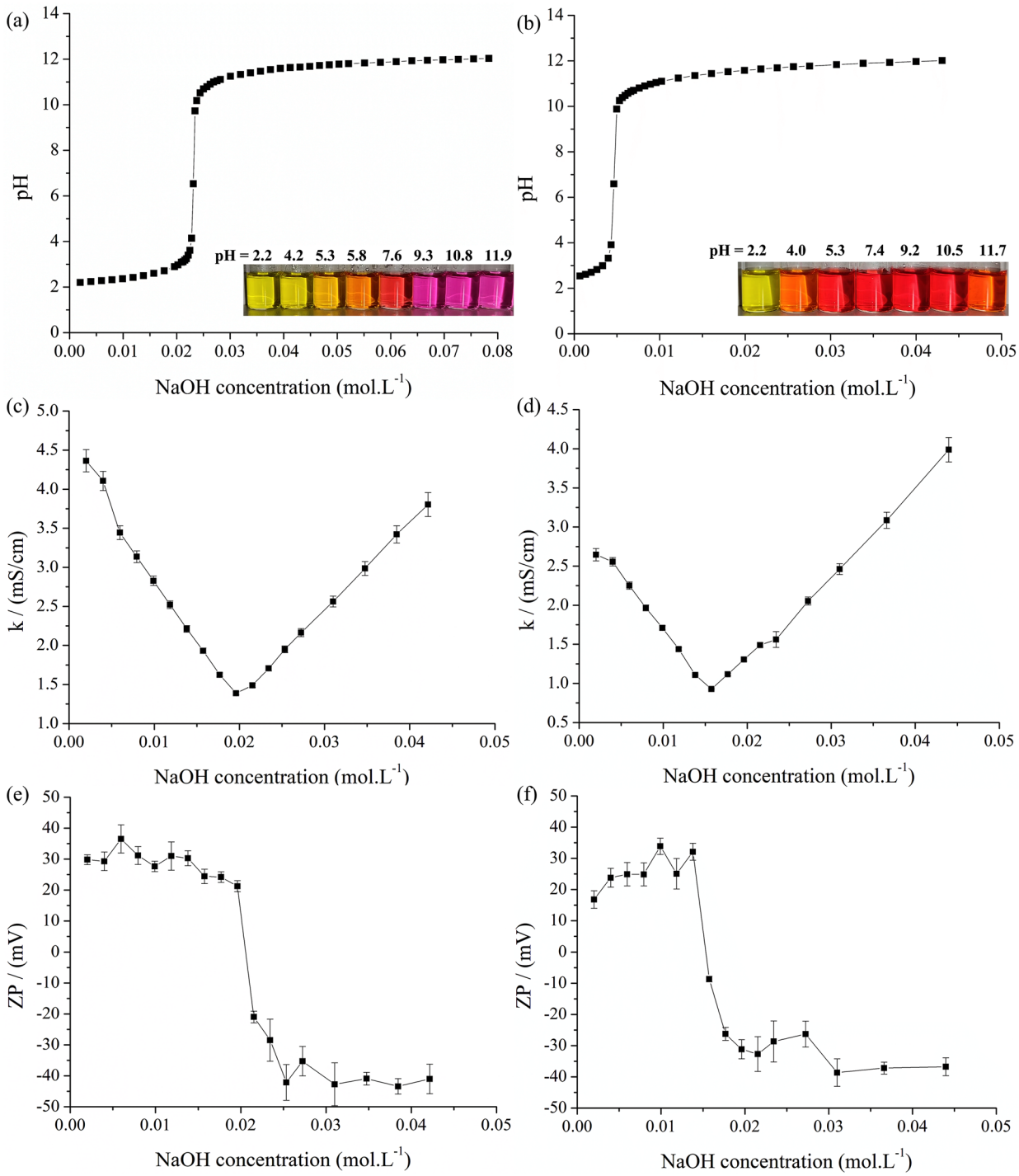

Figure 4: Acid–base titration of (left) SOH and (right) SON utilizing a NaOH 1.0 mol L^{-1} solution. Photos from spiropyrans aqueous solutions were taken at the indicated pHs and are presented in their respective titration curves. NaOH concentration as function of pH (a and b), electrical conductivity (c and d), and zeta potential (e and f).

0.83 ± 0.26 µm for PCL-SON and 0.81 ± 0.29 µm for PCL-SOH, both of which did not significantly varied from pure PCL fibers (Fig. S4), that had a distribution of 0.91 ± 0.29 µm.

Drop shape analysis (insertion Figs. 5 and S5) was also performed to evaluate possible alterations to hydrophobic characteristics of PCL fibers [36] in presence of SON and SOH. PCL-SON was found to have water contact angle of 134.1 ± 1.2° and PCL-SOH 134.7 ± 0.7°. These values confirm their hydrophobic surface property, based on literature data which states contact angle above 90° are characterized as hydrophobic

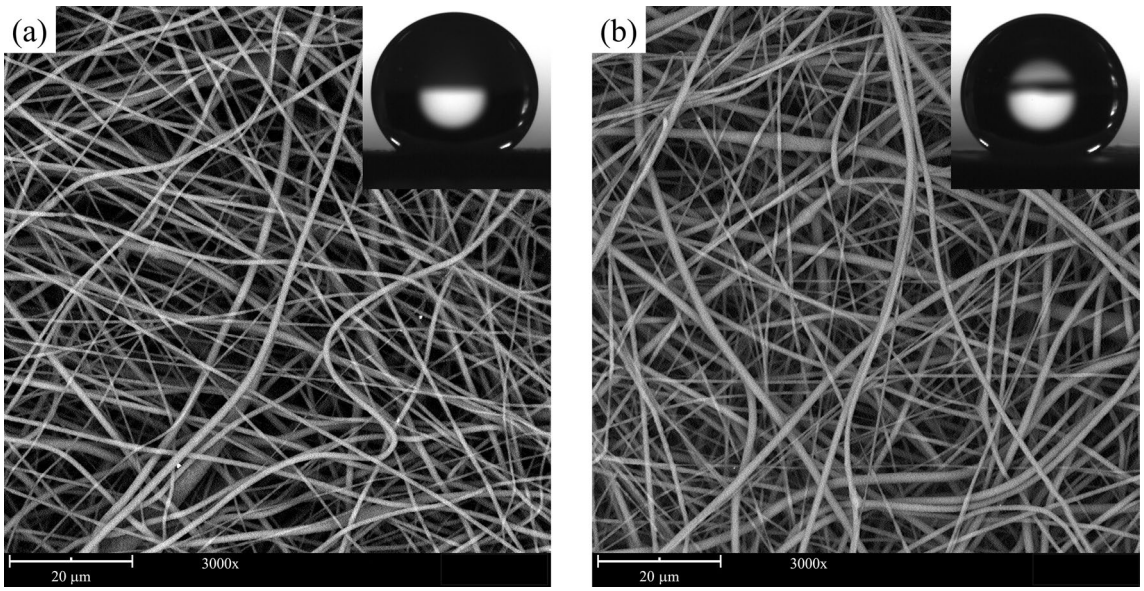

Figure 5: Scanning electron microscopy images at 3.000× for the electrospun fibers of (a) PCL-SON and (b) PCL-SOH. Drop shape analysis images inserted in the top-right corner of each fiber's SEM images.

materials [37]. Both modified fibers presented a slight drop in contact angle values when compared to pure PCL fibers (138.4 ± 0.9°). A decrease in this value was expected considering the spiropyrans in this study are water-soluble, and the fact that the change in the values were not expressive could be an indicative that most of the spiropyrans used in the electrospun process of making the material are not on the surface level of the fibers.

In order to demonstrate the acidochromic properties of the of PCL-SON and PCL-SOH electrospun fibers a setup was assembled as described below. For the acid and base vapor sensing system, the fibers were placed on top of two vials, one with concentrated HCl and one with NH_4OH, as depicted in Fig. 6(a). PCL-SON showed itself as a fast-sensing material for base vapor, quickly changing color with few seconds of exposure. Figure 6(b) displays this color change with 10 s of exposure in the system, which acquires a purplish coloration. With 10 min of exposure this change intensifies and one can also see a change for the acid vapor partition as it lightly darkens the yellow natural color of the fiber [Fig. 6(c)]. As for the PCL-SOH fibers, the color changes do not occur as fast, and so, only the 10 min exposure is shown in Fig. 6(d). Contrary to PCL-SON fibers, the acid vapor gives rise to a more noticeable change in the color of the fibers, as the orange PCL-SOH material transitions to a dark yellow while the base vapor only caused some discoloration circled by a purple ring. These difference in the acid and base sensing could be related to the electron-withdrawing NO_2 group on the phenolate moiety, which makes the PCL-SOH a less acidic material than PCL-SON [33].

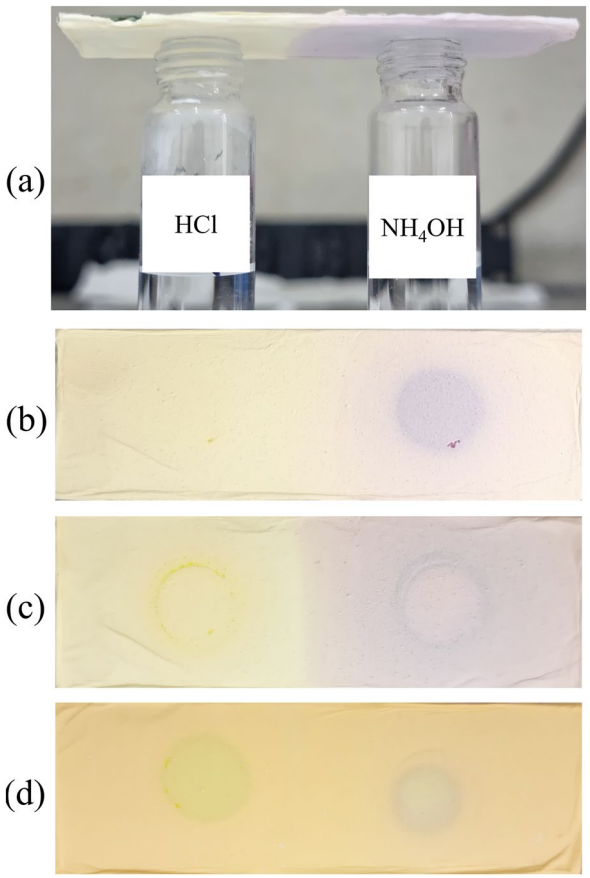

Figure 6: (a) acid/base vapors setup, PCL-SON fibers exposure to HCl 37% and NH_4OH 28% vapors for (b) 10 s and (c) 10 min, and (d) PCL-SOH fibers exposure to HCl and NH_4OH vapors for 10 min.

In order to demonstrate the reversibility electrospun fibers to detect the acid and base vapors glass slides were rotated after approximately 30 s, in which materials color from base vapor was replaced by the acidic color (see movie S1 and movie S2 for PCL-SON and PCL-SOH, respectively). SEM analyses were performed on PCL, as control, PCL-SON and PCL-SOH fibers sample after 30 min of exposure to acid/base vapors (Figure S5). Surprisingly, SEM analysis demonstrated minor morphological differences comparing all three electrospun fibers after exposition to the polymer materials to HCl or NH_4OH vapors. These differences are mainly related to fibers diameter, which decreased after the vapor's exposure, shown in the average distribution and histograms in Figure S6 and Table S2. These results are promising for application of these fibers for concentrated acid and base vapors as a mean to counteract the common hydrolysis drawback of photoacids [38].

Conclusion

Briefly, the two spiropyrans described herein were obtained, structurally and electronically characterized. UV–visible technique allowed the identification of SP, SPH^+, MC, and MCH^+ isomeric species at different pH and with different radiation modes. Raman spectroscopy, a technique that is not commonly used for this class of molecule, allowed us to characterize the photoacids and identify their presence in PCL nanofibers obtained by electrospinning. High surface-to-volume ratio of the polymer matrices provided means to a complete dispersal of the vapors inside the material, characterized by the drastic change in color, in remarkably fast fashion, throughout the entire PCL-SON fiber. On the other hand, PCL-SOH displayed more focused changes related to the vapor setup. The differences observed regarding the response-time of the acid and base sensing, of PCL-SON and PCL-SOH nanofibers, are directly related to the structural and electronical distinct characteristics of the photoacids. However, more detailed studies with resolution techniques could be used to complement these observations, on pH sensitive sensors and for using them for specific applications. Overall, these findings suggest that PCL/photoacids nanofibers can serve as platforms for real time visual detection of concentrated acid and base vapors and that the response of chromic spiropyrans can be controlled and amplified by incorporating with materials with specific morphology and surface area adequate to the sensing field.

Experimental

Reagents and solvents

The following reagents were acquired from Sigma-Aldrich: 2,3,3-trimethylindolenine (98%), 2-hydroxy-5-nitrobenzaldehyde (98%), 2-hydroxybenzaldehyde (≥ 99%), 1,3-propanesultone (98%), diethyl ether (Et_2O) anhydrous (≥ 99.0%), dimethyl sulfoxide-d_6 (DMSO-d_6) (99.9%), acetonitrile (MS grade), and formic acid (≥ 99.0%). The N,N-dimethylformamide (DMF) (> 99.8%) from Êxodo Científica, ammonium hydroxide (28%), sodium hydroxide (> 97.0%), hydrochloric acid (37%), dichloromethane (CH_2Cl_2) (> 99.5%), and ethanol (EtOH) (99.5%) from Quimex, poly-ε-caprolactone (PCL) (MW 43.000) from Polysciences. All reagents were used without further purification.

Synthesis of SON and SOH spiropyrans

Both spiropyrans (SOH and SON) were synthesized according to the literature [9]. Briefly, 2,3,3-trimethylindolenine (for SOH 3.24 g, 0.02 mmol, for SON 2.94 g, 0.018 mol) was added into 1,3-propanesultone (for SOH 2.46 g, 0.02 mol, for SON 2.26 g, 0.018 mol). The mixtures were stirred at 90 °C for 4 h under N_2 atmosphere. The product is a purple solid which was filtered and washed with cold diethyl ether (for SOH, 5.13 g, 90% yield, for SON 4.41 g, 85% yield). For SOH, 2,3,3-trimethyl-1-(3-sulfonatepropyl)-3*H*-indolium (5.13 g, 0.018 mol) and 2-hydroxybenzaldehyde (2.23 mg, 0.018 mol) were added into anhydrous ethanol (5 mL). The solution was kept under reflux for 16 h. The orange solid was obtained by filtration (5.19 g, 74% yield). For SON, 2,3,3-trimethyl-1-(3-sulfonatepropyl)-3*H*-indolium (4.41 g, 0.015 mol) and 2-hidroxy-5-nitrobenzaldehyde (2.62 mg, 0.015 mol) were added into anhydrous ethanol (5 mL). The solution was kept under reflux for 16 h. The green solid was obtained by filtration (5.25 g, 78% yield).

Structural characterization of SON and SOH spiropyrans and electrospun fibers

The Raman spectra of the spiropyrans and polymer fibers samples were collected on an RFS 100 FT-Raman Bruker spectrometer equipped with a germanium detector using liquid nitrogen as the coolant and excited with a 1064 nm beam from an NdYAG laser. Sample was placed into a small aluminum sample cup; the laser light, with a power of 50–100 mW, was introduced and focused on the sample, and the scattered radiation was collected at 180°. For each spectrum, an average of 256 scans were collected at a resolution of 4 cm^{-1} over the range of 4000–400 cm^{-1}. Each spectrum was obtained at least twice to guarantee reproducibility of intensity and wavenumber position. NMR experiments were carried out using a Bruker ONEBAY ASCEND 400 at a resonance frequency of 400 MHz at 27 °C and in a quartz tube of 5 mm. SON and SOH (5.0 mg of each sample) were dissolved in DMSO-d_6 as solvent and homonuclear and heteronuclear experiments conduct in order to attribute the molecule chemical shifts. Mass analyses were carried out in a 6530 Accurate-Mass Q-TOF system equipped with Dual AJS ESI source and a 1260 Infinity II High-Performance Liquid Chromatography instrument as

injection system both from Agilent Technologies (Palo Alto, CA, USA). During the analyses the room temperature at 23 °C was controlled through air conditioning. The room humidity level was monitored by a Digital Thermo-Hygrometer and remained within the range of 56–60%. Before analyses was performed a mass calibration using Agilent calibrant solution in Standard (3200 m/z) Extended Dynamic Range (2 GHz) mode followed by MS system cleaning with a commercial high-performance liquid chromatography (HPLC) flush solution containing acetonitrile, cyclohexane, dichloromethane, and isopropyl alcohol, using a flow of 0.4 mL min^{-1} for 15 min. Each sample (15.0 µL) was directly injected through the HPLC system using a mobile phase consisted of acetonitrile and formic acid (99.5:0.5% v/v) at 0.4 mL min^{-1} flow rate. The data were collected in positive ESI mode operated in full scan from m/z 100–1000 at 1 spectra/sec scan rate. The capillary voltage was fitted at + 3.5 kV and the fragmentor voltage was set at 70 V. The nebulizer pressure was kept at 50 psig, drying gas at 350 °C with 12 L min^{-1} flow rate and sheath gas at 325 °C with 11 L min^{-1} flow rate.

UV–visible analysis of SON and SOH spiropyrans

All UV–visible absorption spectra were obtained at 20 ± 1 °C. Spectra were measured in the UV–visible range (from 200 to 800 nm) using a Varian Cary 50 Scan spectrophotometer and quartz cuvettes with a path length of 10 mm and 1.5 mL. Solutions of different pH were obtained with addition of HCl or NaOH at 1.0 mol L^{-1} solution.

Spiropyrans acid/base titrations

SON (at 0.16 mmol L^{-1}) or SOH (at 0.18 mmol L^{-1}) spiropyrans were dissolved in Milli-Q® water and then these solutions were acidified using HCl to pH 2.2 for SOH and 2.5 for SON. Then, NaOH aliquots were added, and pH measured to 12.0. Similar titrations were carried out in order to acquire electrical conductivity (k) and zeta potential (ZP) measurements. The ZP values were obtained through electrophoretical mobility (EM) measurements using Smoluchowski equation [39]. The EM was, in turn, determined by means of the laser doppler micro-electrophoresis technique, at scattering angle of 173° using a Malvern Zetasizer Nano ZS apparatus. Simultaneously, k values were also obtained. Titration and homogenization were performed at stirring speed of 150 rpm using a magnetic stirrer at 27 °C. Immediately after each injection of titrant, the samples were withdrawn with a syringe, and inserted in a disposable cell folded capillary (DPS1060) where their ZP and k were measured at 25 °C, after 30 s of equilibration time using a peltier system coupled in Zetasizer. The ZP and k values were determined by the average of five independent measurements, each obtained as the mean of 10 counts.

TABLE 1: Parameters used to obtain PCL electrospun fibers and those containing SOH or SON.

Fibers	Flow rate solution [mL h^{-1}]	Collector distance [cm]	DC voltage [kV]
PCL	5	19	15
PCL-SOH-2.0%	1.3–2.0	12–18	10–14
PCL-SON-2.0%	1.2–2.0	13–19	11–14

Electrospinning process

PCL fibers were prepared using a solution of 30%w in DMF/DCM (at 8.5:1.5 vol) containing 2.0% wt of SON (PCL-SON) or SOH, (PCL-SOH). All fibers were obtained using a Harvard Apparatus PHD 2000 infusion pump and a Gamma High Voltage, voltage generator. The electrospinning parameters are presented in Table 1.

Fibers' characterization and properties

The morphology observations and chemical microanalyses of the polymer fibers were conducted by scanning electron microscopy (SEM, Phenom ProX, ThermoFischer Scientific). The SEM mode used was BSE (Back-scattered Electron Detector), operated at 10 kV, with 3.000 × magnification, for all samples no previous treatment, such as metal coating, was necessary. The diameters for all fibers were measured from SEM images using at least 20 measurements from each three different micrographs, using ImageJ 1.52a version analysis software. The hydrophobicity of the fibers was investigated on the upper surface of the electrospun fiber mats using a contact angle measuring system G10 (Krüss GmbH, Germany) by means of sessile drop method, at room temperature, using 10 × 5 µL drops of ultrapure water (Milli-Q® water) for each fiber sample. The values presented in the discussion section were obtained by standard deviation and arithmetic mean calculations of the 10 angles obtained from the analysis. For the acid and base vapor sensing photos, PCL-SON and PCL-SOH fibers (with 0.1 mm thickness) were collected on microscopic slides and placed facing two glass vials containing 5 mL of hydrochloric acid (HCl) 37% and 5 mL of ammonium hydroxide (NH_4OH) 28% for varying periods of time. Photos and videos were taken using the Samsung Galaxy S21 Ultra's back-facing camera with 108 megapixels resolution for photos and 1440 × 1440 resolution for videos.

Acknowledgments

This work was supported by CNPq (Grant Nos. 431133/2018-2; 437418/2018-9; 308278/2020-8; 309720/2020-6 and scholarship 157706/2019-2) and FAPEMIG (Grant Nos. APQ-01293-14; APQ 02052/21 and APQ-00210-21) and FINEP

(CT-INFRA 01/2013-REF 0633/13). This work was also supported by Biosmart Nanotechnology Ltda agreement with UNIFEI (process number 23088.015061/2019-72). Authors would like to thank LIPq-LAREMAR facilities from Department of Chemistry from UFMG for NMR support.

Data availability

Derived data supporting the findings of this study are available from the corresponding author on request.

Declarations

Conflict of interest The authors declare that they have no conflict of interest.

Supplementary Information

The online version contains supplementary material available at https://doi.org/10.1557/s43578-022-00842-5.

References

1. L. Kortekaas, W.R. Browne, The evolution of spiropyran: fundamentals and progress of an extraordinarily versatile photochrome. Chem. Soc. Rev. **48**(12), 3406 (2019)
2. M. Natali, L. Soldi, S. Giordani, A photoswitchable Zn (II) selective spiropyran-based sensor. Tetrahedron **66**(38), 7612 (2010)
3. F. Khakzad, A.R. Mahdavian, H. Salehi-Mobarakeh, A. Rezaee Shirin-Abadi, M. Cunningham, Redispersible PMMA latex nanoparticles containing spiropyran with photo-, pH- and CO2-responsivity. Polymer (Guild) **101**, 274 (2016)
4. F.B. Miguez, I.F. Reis, L.P. Dutra, I.M.S. Silva, T. Verano-Braga, J.F. Lopes, F.B. De Sousa, Electronic investigation of light-induced reversible coordination of Co(II)/spiropyran complex. Dye. Pigment. **171**, 107757 (2019)
5. V.I. Minkin, Photo-, thermo-, solvato-, and electrochromic spiroheterocyclic compounds. Chem. Rev. **104**(5), 2751 (2004)
6. H. Zhang, Y. Chen, Y. Lin, X. Fang, Y. Xu, Y. Ruan, W. Weng, Spiropyran as a mechanochromic probe in dual cross-linked elastomers. Macromolecules **47**(19), 6783 (2014)
7. M. Bletz, U. Pfeifer-Fukumura, U. Kolb, W. Baumann, Ground- and first-excited-singlet-state electric dipole moments of some photochromic spirobenzopyrans in their spiropyran and merocyanine form. J. Phys. Chem. A **106**(10), 2232 (2002)
8. I. Panaiotov, S. Taneva, A. Bois, F. Rondelez, Photoinduced dilatational motion in monolayers of poly(methyl methacrylate) having benzospiropyran side groups. Macromolecules **24**(15), 4250 (1991)
9. Z. Shi, P. Peng, D. Strohecker, Y. Liao, Long-lived photoacid based upon a photochromic reaction. J. Am. Chem. Soc. **133**(37), 14699 (2011)
10. M. Schnurbus, M. Kabat, E. Jarek, M. Krzan, P. Warszynski, B. Braunschweig, Spiropyran sulfonates for photo- and pH-responsive air-water interfaces and aqueous foam. Langmuir **36**(25), 6871 (2020)
11. C. Berton, D.M. Busiello, S. Zamuner, R. Scopelliti, F. Fadaei-Tirani, K. Severin, C. Pezzato, Light-switchable buffers. Angew. Chemie Int. Ed. **60**(40), 21737 (2021)
12. G. Kocak, C. Tuncer, V. Bütün, PH-responsive polymers. Polym. Chem. **8**(1), 144 (2017)
13. M. Wei, Y. Gao, X. Li, M.J. Serpe, Stimuli-responsive polymers and their applications. Polym. Chem. **8**(1), 127 (2017)
14. M. Sponchioni, U. Capasso Palmiero, D. Moscatelli, Thermo-responsive polymers: applications of smart materials in drug delivery and tissue engineering. Mater. Sci. Eng. C **102**, 589 (2019)
15. S. Pedron, S. Van Lierop, P. Horstman, R. Penterman, D.J. Broer, E. Peeters, Stimuli responsive delivery vehicles for cardiac microtissue transplantation. Adv. Funct. Mater. **21**(9), 1624 (2011)
16. A.S. Hoffman, Stimuli-responsive polymers: biomedical applications and challenges for clinical translation. Adv. Drug Deliv. Rev. **65**(1), 10 (2013)
17. A. Richter, G. Paschew, S. Klatt, J. Lienig, K.F. Arndt, H.J.P. Adler, Review on hydrogel-based pH sensors and microsensors. Sensors **8**(1), 561 (2008)
18. M. Mrinalini, S. Prasanthkumar, Recent advances on stimuli-responsive smart materials and their applications. ChemPlusChem **84**(8), 1103 (2019)
19. F. Arab Hassani, Q. Shi, F. Wen, T. He, A. Haroun, Y. Yang, Y. Feng, C. Lee, Smart materials for smart healthcare—moving from sensors and actuators to self-sustained nanoenergy nanosystems. Smart Mater. Med. **1**, 92 (2020)
20. F.B. De Sousa, F. Alexis, S. Giordani, Editorial: photochromic materials: design and applications. Front. Mater. (2021). https://doi.org/10.3389/fmats.2021.720172
21. M.E. Genovese, A. Athanassiou, D. Fragouli, Photoactivated acidochromic elastomeric films for on demand acidic vapor sensing. J. Mater. Chem. A **3**(44), 22441 (2015)
22. J. Keyvan Rad, A.R. Ghomi, K. Karimipour, A.R. Mahdavian, Progressive readout platform based on photoswitchable polyacrylic nanofibers containing spiropyran in photopatterning with instant responsivity to acid-base vapors. Macromolecules **53**(5), 1613 (2020)
23. A. Steinegger, O.S. Wolfbeis, S.M. Borisov, Optical sensing and imaging of pH values: spectroscopies, materials, and applications. Chem. Rev. **120**(22), 12357 (2020)
24. R. Avolio, A. Grozdanov, M. Avella, J. Barton, M. Cocca, F. De Falco, A.T. Dimitrov, M.E. Errico, P. Fanjul-Bolado, G. Gentile, P. Paunovic, A. Ribotti, P. Magni, Review of pH sensing materials from macro- to nano-scale: recent developments and examples of seawater applications. Crit. Rev. Environ. Sci. Technol. (2020). https://doi.org/10.1080/10643389.2020.1843312

25. M.E. Genovese, E. Colusso, M. Colombo, A. Martucci, A. Athanassiou, D. Fragouli, Acidochromic fibrous polymer composites for rapid gas detection. J. Mater. Chem. A **5**(1), 339 (2017)
26. R. Klajn, Spiropyran-based dynamic materials. Chem. Soc. Rev. **43**(1), 148 (2014)
27. S. Huang, K. Wang, S. Wang, Y. Wang, M. Wang, Highly fluorescent polycaprolactones with tunable light emission wavelengths across visible to NIR spectral window. Adv. Mater. Interfaces **3**(17), 1600259 (2016)
28. R.C.L. Machado, F. Alexis, F.B. De Sousa, Nanostructured and photochromic material for environmental detection of metal ions. Molecules **24**(23), 4243 (2019)
29. I.F. Reis, F.B. Miguez, C.A.A. Vargas, T.G. Menzonatto, I.M.S. Silva, T. Verano-Braga, J.F. Lopes, T.A.S. Brandão, F.B. De Sousa, Structural and electronic characterization of a photoresponsive lanthanum(III) complex incorporated into electrospun fibers for phosphate ester catalysis. ACS Appl. Mater. Interfaces. (2020). https://doi.org/10.1021/acsami.0c03571
30. C. Berton, D.M. Busiello, S. Zamuner, E. Solari, R. Scopelliti, F. Fadaei-Tirani, K. Severin, C. Pezzato, Thermodynamics and kinetics of protonated merocyanine photoacids in water. Chem. Sci. **11**(32), 8457 (2020)
31. D. Lin-Vien, N.B. Colthup, W.G. Fateley, J.G. Grasselli, *The handbook of infrared and Raman characteristic frequencies of organic molecules* (Elsevier, Amsterdam, 1991), pp. 477–490
32. A.P. Kotula, C.R. Snyder, K.B. Migler, Determining conformational order and crystallinity in polycaprolactone via Raman spectroscopy. Polymer (Guildf) **117**, 1 (2017)
33. Y. Liao, Design and applications of metastable-state photoacids. Acc. Chem. Res. **50**(8), 1956 (2017)
34. J. Morais de Faria, L. Alkimin Muniz, J.F.Z. Netto, D. Scheres Firak, F.B. De Sousa, F. da Silva Lisboa, Application of a hybrid material formed by layered zinc hydroxide chloride modified with spiropyran in the adsorption of Ca^{2+} from water. Colloids Surfaces A Physicochem. Eng. Asp. **631**, 127738 (2021)
35. A. Julià-López, J. Hernando, D. Ruiz-Molina, P. González-Monje, J. Sedó, C. Roscini, Temperature-controlled switchable photochromism in solid materials. Angew. Chem. Int. Ed. **55**(48), 15044 (2016)
36. M.C.R. Simões, S.M. Cragg, E. Barbu, F.B. De Sousa, The potential of electrospun poly(methyl methacrylate)/polycaprolactone core–sheath fibers for drug delivery applications. J. Mater. Sci. **54**(7), 5712 (2019)
37. L.M. Jenkins, A.M. Donald, Contact angle measurements on fibers in the environmental scanning electron microscope. Langmuir **15**, 7829 (1999)
38. N. Abeyrathna, Y. Liao, Stability of merocyanine-type photoacids in aqueous solutions. J. Phys. Org. Chem. **30**(8), e3664 (2017)
39. R. Xu, Methods to resolve mobility from electrophoretic laser light scattering measurement. Langmuir **9**(11), 2955 (1993)